Characterisation of Sm^{2+}-doped CsYbBr$_3$, CsYbI$_3$ and YbCl$_2$ for near-infrared scintillator application

van Aarle, Casper; Krämer, Karl W.; Dorenbos, Pieter

Important note
To cite this publication, please use the final published version (if applicable).
Please check the document version above.

Full Length Article

Characterisation of Sm^{2+}-doped $CsYbBr_3$, $CsYbI_3$ and $YbCl_2$ for near-infrared scintillator application

Casper van Aarle [a,*], Karl W. Krämer [b], Pieter Dorenbos [a]

[a] *Delft University of Technology, Faculty of Applied Sciences, Department of Radiation Science and Technology, Section Luminescence Materials, Mekelweg 15, 2629, JB, Delft, the Netherlands*
[b] *University of Bern, Department of Chemistry and Biochemistry, Freiestrasse 3, CH-3012, Bern, Switzerland*

ARTICLE INFO

ABSTRACT

Fast energy transfer from Yb^{2+} to Sm^{2+} is a requirement when using Yb^{2+} as a sensitiser for Sm^{2+} emission for near-infrared scintillator applications. This cannot be achieved through dipole-dipole interactions due to the spin-forbidden nature of the involved Yb^{2+} transition, making the rate of energy transfer too slow for application. This work explores whether exploiting the exchange interaction by increasing the Yb^{2+} concentration to 99% is an effective way to increase the rate at which energy is transferred from Yb^{2+} to Sm^{2+}. The scintillation characteristics of $CsYbBr_3$:1%Sm, $CsYbI_3$:1%Sm and $YbCl_2$:1%Sm single crystals were studied through ^{137}Cs excited pulse height spectra, X-ray excited decay and X-ray excited luminescence spectra. An energy resolution of 7% and a light yield of 30,000 ph/MeV was achieved with $CsYbI_3$:1%Sm. Photoluminescence spectroscopy and decay studies were performed to study the band structure and relaxation dynamics.

1. Introduction

The energy resolution of a scintillator is an important parameter, as it is a measure for how accurately the energy deposited in a scintillation event can be determined [1,2]. It is most commonly defined as the full width at half maximum of the photopeak of ^{137}Cs 662 keV γ-ray detection in a pulse height spectrum. The current best energy resolution was achieved with $LaBr_3$:Ce,Sr, in which the resolution of 2.0% is close to the fundamental limit determined by photon statistics [3]. Its emission wavelength is around 375 nm, which is where most photomultiplier tubes (PMT) have maximum quantum efficiency. As long as scintillation photons cannot be detected with higher efficiency, the only way to go below 2% energy resolution is developing scintillators with a light yield higher than the 70,000 ph/MeV of $LaBr_3$:Ce,Sr.

Some Eu^{2+} doped halides are reported to have such high light yields. For example SrI_2:Eu and $CsBa_2I_5$:Eu have been reported to emit close to 100,000 ph/MeV and energy resolutions of 2.6% and 2.3% have been achieved with these compounds, respectively [4–9]. However, the drawback of these scintillators is that an Eu^{2+} emission photon can often be reabsorbed by other Eu^{2+} ions that the photon encounters when travelling through the crystal [7,10–13]. This makes Eu^{2+} doped halides less suitable for applications that require large sized crystals. In order to

find a scintillator that truly surpasses $LaBr_3$:Ce,Sr, a scintillator must be found that does not have the self-absorption problem of Eu^{2+}.

Sm^{2+} is a possible candidate as a dopant for such a scintillator. When doped in iodides, its $4f^55d \rightarrow 4f^6$ emission lies typically between 720 nm and 900 nm, which can be detected with an avalanche photodiode (APD) with near 100% quantum efficiency [14]. Its decay time is usually around 2 μs [15,16], which is fast enough for application in γ-ray spectroscopy. The $4f^55d \rightarrow 4f^6$ transition of Sm^{2+} can end up on any of the $4f^6[^7F_J]$ states, while absorption only takes place from the $4f^6[^7F_0]$ ground state. Because of this, Sm^{2+} doped scintillators experience less self-absorption than their Eu^{2+} doped counterparts [17]. Due to its broad absorption bands across the entire visible spectrum, Sm^{2+} can easily be sensitised by other lanthanides. Dopants with which high light yields have previously been achieved can thus be used to excite Sm^{2+}. Awater et al. have demonstrated that Eu^{2+} excitations can be transferred efficiently to Sm^{2+} in SrI_2 [17]. Eu^{2+} was later used as a scintillation sensitiser by Wolszczak et al. with which an energy resolution of 3.2% was attained in $CsBa_2I_5$:2%Eu,1%Sm [18]. Other attempts have been made using $CsSrI_3$ and $BaBrI$ as host materials [19].

Recently, Yb^{2+} has gained in popularity as a potential alternative to Eu^{2+} as activator for inorganic scintillators [20–24]. Yb^{2+} in the ground state has a full $4f^{14}$ subshell, which means it has no 4f-4f transitions and

the first excited state is of the $4f^{13}5d$ configuration. The spin-orbit coupling of the $4f^{13}$ electrons causes splitting of the $4f^{13}5d$ level into two $4f^{13}[^2F_J]5d$ levels, with $J = 7/2$ or $J = 5/2$. The latter lies at approximately 10,000 cm^{-1} higher energy. The crystal field interaction with the 5d causes splitting into 5 energy levels, labelled $5d_n$ with $n = 1$–5. The exchange interaction between the $4f^{13}$ electrons and the electron in 5d causes further splitting into states with spin $S = 0$ or $S = 1$, referred to as the $4f^{13}[^2F_J]5d_n[LS]$ and $4f^{13}[^2F_J]5d_n[HS]$ states, respectively. The size of the exchange splitting is approximately 2000 cm^{-1}, with the [LS] state lying at highest energy [25].

Yb^{2+} emission is mostly observed from the spin-forbidden $4f^{13}[^2F_{7/2}]5d_1[HS] \rightarrow 4f^{14}$ transition. When thermal relaxation from the $4f^{13}[^2F_{7/2}]5d_1[LS]$ to $4f^{13}[^2F_{7/2}]5d_1[HS]$ state is slow enough, spin-allowed $4f^{13}[^2F_{7/2}]5d_1[LS] \rightarrow 4f^{14}$ emission is also observed. The decay times of these emissions are typically around 1 µs for the spin-allowed emission and 1 ms for the spin-forbidden emission [26], the latter being too slow for scintillator applications as it imposes a severe limitation on the maximum achievable count rate.

We recently studied the feasibility of using Yb^{2+} as a scintillation sensitiser for Sm^{2+} in CsBa$_2$I$_5$ [27]. It was found that energy transfer from Yb^{2+} to Sm^{2+} takes place through the dipole-dipole interaction and energy can be transferred from both the Yb^{2+} $4f^{13}[^2F_{7/2}]5d_1[HS]$ and $4f^{13}[^2F_{7/2}]5d_1[LS]$ states. As the rate of energy transfer through dipole-dipole interactions scales with the oscillator strength of the involved transitions [28], energy transfer to Sm^{2+} from the Yb^{2+} $4f^{13}[^2F_{7/2}]5d_1[HS]$ state is about 200 times slower than that from the $4f^{13}[^2F_{7/2}]5d_1[LS]$ state. This resulted in an unwanted slow component in the decay of the Sm^{2+} $4f^55d \rightarrow 4f^6$ emission. It was concluded that where Yb^{2+} doped scintillators are held back by the long decay time of the spin-forbidden $4f^{13}[^2F_{7/2}]5d_1[HS] \rightarrow 4f^{14}$ transition, scintillators that use Yb^{2+} as a scintillation sensitiser suffer from the same problem.

In this work a solution for the slow energy transfer from Yb^{2+} to Sm^{2+} is explored. The rate of radiationless energy transfer from one ion to another scales strongly with the distance R between the two ions. In the case of the dipole-dipole interaction, the rate scales with R^{-6}, whereas the exchange interaction scales as $\exp(-2R/L)$, where L is approximately the Bohr radius of the involved ions [28]. If the Yb^{2+} excitations are located close enough to a Sm^{2+} ion, the rate of energy transfer to Sm^{2+} is much faster. To achieve this, single crystals of CsYbBr$_3$:1%Sm, CsYbI$_3$:1%Sm and YbCl$_2$:1%Sm are studied, which can be viewed as materials in which the Yb^{2+} doping concentration is increased to 99%. CsYbBr$_3$ (CaTiO$_3$ type structure) and CsYbI$_3$ (GdFeO$_3$ type structure) have perovskite structures similar to those of CsCaBr$_3$ and CsCaI$_3$, in which the Yb^{2+} site has a coordination number of 6 [29, 30]. YbCl$_2$ has a SrI$_2$ type structure where the Yb^{2+} site has a coordination number of 7 [31]. The aim is that the short distance between neighbouring Yb^{2+} ions allows for migration of excitations towards Sm^{2+}.

The energy transfer process is shown schematically in Fig. 1. Arrow 1 depicts the excitation of an Yb^{2+} ion. Arrows 2 and 3 depict energy transfer over neighbouring Yb^{2+} ions. Due to the forbidden nature of the Yb^{2+} $4f^{13}[^2F_{7/2}]5d_1[HS] \rightarrow 4f^{14}$ transition, it is expected that the exchange mechanism plays a large role in the migration of Yb^{2+} excitations. Arrow 4 corresponds to the energy transfer from an Yb^{2+} ion to a Sm^{2+} ion, after which energy is lost through thermal relaxation to the lowest energy $4f^55d$ state along arrow 5. Due to the energy loss in the thermal relaxation process, the excitation cannot be transferred back to Yb^{2+}. Finally, Sm^{2+} emission is observed as indicated by arrow 6.

In addition to solving the problem of slow energy transfer from Yb^{2+} to Sm^{2+}, there may be other benefits to using such high Yb^{2+} concentrations. The high Z number and small ionic radius of Yb^{2+} allows to create crystals with more γ-photon stopping power than most Ln^{2+} doped halide scintillators. Additionally, the $4f^{14}$ ground state of Yb^{2+} lies within the band gap. This reduces the minimal energy required to excite an electron to the conduction band and could potentially result in the emission of more photons per absorbed γ-ray energy.
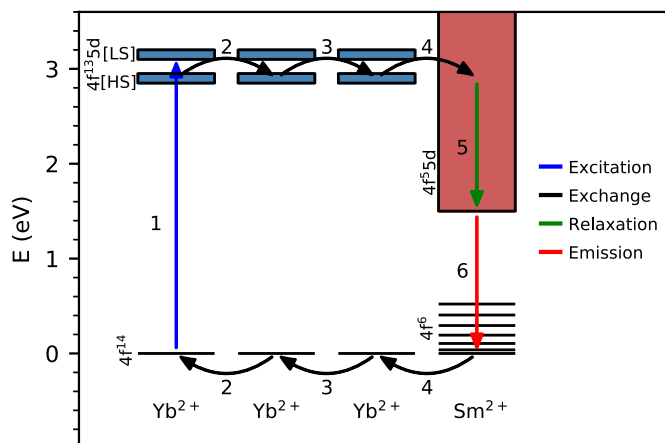

Fig. 1. Schematic of the energy transfer processes from Yb^{2+} to Sm^{2+}. After initial excitation of an Yb^{2+} ion, the excitation energy migrates over neighbouring Yb^{2+} ions until it is transferred to Sm^{2+} from which emission is observed. The energy scale on the y-axis corresponds to approximate values for the samples studied in this work.

To assess the scintillation performance of the samples, the temperature stability of the scintillators is determined through X-ray excited emission spectra at temperatures ranging from 78 K to 700 K. The room temperature decay times are measured to determine whether the scintillation pulses are fast enough for application. ^{137}Cs excited pulse height spectra have been taken to determine the energy resolution and light yield. Photoluminescence excitation and emission spectra and decay time profiles have been measured to study energy transfer from Yb^{2+} to Sm^{2+}.

2. Experimental techniques

CsYbBr$_3$:1%Sm^{2+}, CsYbI$_3$:1%Sm^{2+}, and YbCl$_2$:1%Sm^{2+} crystals were grown from the binary halides by the vertical Bridgman technique. CsBr (5 N, Alfa) and CsI (Merck, suprapur) were dried in high vacuum at 200 °C. YbX$_3$ with X = Cl, Br were prepared by the ammonium halide method [32]. Yb$_2$O$_3$ (6 N, Metall Rare Earth Ltd.) and NH$_4$X (Merck, p. a., sublimed) were dissolved in HX acid (Merck, suprapur) to yield a ternary ammonium rare earth halide, which was dried and decomposed to the YbX$_3$ halide by heating in vacuum, see equation (1).

$$Yb_2O_3 + 7\,NH_4X + HX \rightarrow (NH_4)_3YbX_6 \rightarrow YbX_3 \qquad (1)$$
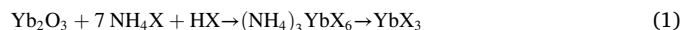
For the removal of YbOX traces the YbX$_3$ halide was sublimed in a sealed Au ampoule in vacuum at 960 °C for YbCl$_3$ and 800 °C for YbBr$_3$. Subsequently, the halide was reduced by Yb metal in a Ta ampoule according to equation (2).

$$2\,YbX_3 + Yb \rightarrow 3\,YbX_2 \qquad (2)$$

The Ta ampoule was sealed under vacuum into a silica ampoule and kept 1 day at 900 °C and 7 days at 750 °C for YbCl$_2$ and 1 day at 970 °C and 7 days at 700 °C for YbBr$_2$.

YbI$_2$ was prepared from the elements in a silica ampoule sealed under vacuum. Yb (4 N, Metall Rare Earth Ltd.) and I$_2$ (Merck, p. a., sublimed) were slowly heated to 650 °C. One end of the ampoule protruded from the tube furnace to avoid high iodine pressure during the reaction. After the reaction was finished, the ampoule was opened and heated in vacuum to remove excess I$_2$. The product was sealed in a silica ampoule and purified by Bridgman crystal growth starting at 790 °C.

The samarium halides were prepared by the same methods as described above for ytterbium. SmX$_3$ were synthesized from Sm$_2$O$_3$ (3 N, Fluka). SmCl$_3$ was sublimed at 600 °C and SmBr$_3$ at 650 °C in high vacuum. SmCl$_2$ was prepared at 650 °C and SmBr$_2$ at 700 °C using Sm (3 N, Alfa). SmI$_3$ was prepared at 700 °C and sublimed for purification in a

silica ampoule under vacuum at 800 °C. The reduction to SmI_2 took place in a Ta ampoule 1 day at 900 °C and 7 days at 600 °C.

The crystal growth was done using a moving furnace and a static ampoule. The stoichiometric mixture of the starting materials was sealed in a Ta ampoule under He by arc welding. The material was molten at 740 °C for $YbCl_2$:1% Sm^{2+}, 680 °C for $CsYbBr_3$:1%Sm^{2+}, and 760 °C for $CsYbI_3$:1%Sm^{2+}. After one day at this temperature, the crystal was grown by moving up the furnace with 0.1 mm/min. During about ten days the sample reached room temperature. Crystals were cleaved from the boules for spectroscopic investigations. The denoted doping level represents the melt composition. Since starting materials and products are highly hygroscopic and sensitive to oxidation, all handling was done under strictly dry and oxygen-free conditions (H_2O and $O_2 < 0.1$ ppm) in glove boxes and sealed sample containers.

X-ray excited luminescence spectra have been measured using an X-ray tube with tungsten anode operated at 79 kV as excitation source. Low energy X-rays were filtered out to avoid radiation damage at the sample surface. The sample was attached to the cold finger of a Janis VPF-700 cryostat. The emission from the sample face of incident X-ray excitation was coupled into an optical fibre and read out with an Ocean Insights QE Pro spectrometer. The optical fibre entrance was placed under a 90°angle with the X-ray tube.

Pulse height spectra were measured with a windowless Advanced Photonix APD (type 630-70-72-510) operated with a 1690 V bias. The temperature of the APD was stabilised at 260 K with two Peltier coolers connected to a Lakeshore 331 temperature controller. The APD output signal was amplified by a Cremat CR-112 pre-amplifier before going into an Ortec 672 spectroscopic amplifier, after which it was read out with an Ortec 926 analog-to-digital converter. The sample was positioned above the PMT surrounded with PTFE powder, using the pressed powder method described by de Haas and Dorenbos [14]. Light yields were determined by comparing the position of the photopeak with the peak generated by 17.8 keV X-rays of [241]Am being directly detected by the APD.

X-ray excited decay curves were measured using a time correlated single photon counting method. A PicoQuant LDH-P-C-400 M laser diode exciting a Hamamatsu N5084 light excited X-ray tube with tungsten anode operated at 40 kV was used as excitation source. The sample was attached to the cold finger of a Janis VPF-700 cryostat. The sample chamber was kept at a pressure of 10^{-5} mbar to protect hygroscopic samples from exposure to moisture. The scintillation light was detected using an ID Quantique ID100-50 single-photon detector, generating a stop signal. The start and stop signals were processed using an Ortec 567 time-to-amplitude converter of which the output was connected to an Ortec 413 CE Quad 8 k analog-to-digital converter.

The photoluminescence emission and excitation spectra were measured using a 450 W Xenon lamp as light source. The excitation light passed through a Horiba Gemini 180 monochromator before entering the sample chamber. The emission light from the sample passed through a Princeton Instruments SpectraPro-SP2358 monochromator before being detected by a Hamamatsu R7600-20 PMT. An optical filter was placed between the sample chamber and the emission monochromator to filter out the excitation light. The sample was attached to the cold finger of a closed cycle Helium cryostat.

The photoluminescence decay was measured with an EKSPLA NT230 OPO laser as excitation source. The emission light from the sample passed through a Princeton Instruments SpectraPro-SP2358 monochromator before being detected by a Hamamatsu R7600-20 PMT. The PMT output was read out using a CAEN DT5730 digitiser.

3. Results

Fig. 2a shows the X-ray excited emission spectra of $CsYbBr_3$:1%Sm between 78 K and 700 K. The sample shows broad band emission between 600 nm and 950 nm. Based on comparison with the Eu^{2+} $4f^65d \rightarrow 4f^7$ emission in $CsCaBr_3$:Eu located at 433 nm [33], the Sm^{2+} $4f^55d \rightarrow 4f^6$ emission is expected at a wavelength of 796 nm [25]. Therefore, the broad emission band is assigned to the Sm^{2+} $4f^55d \rightarrow 4f^6$ emission. As
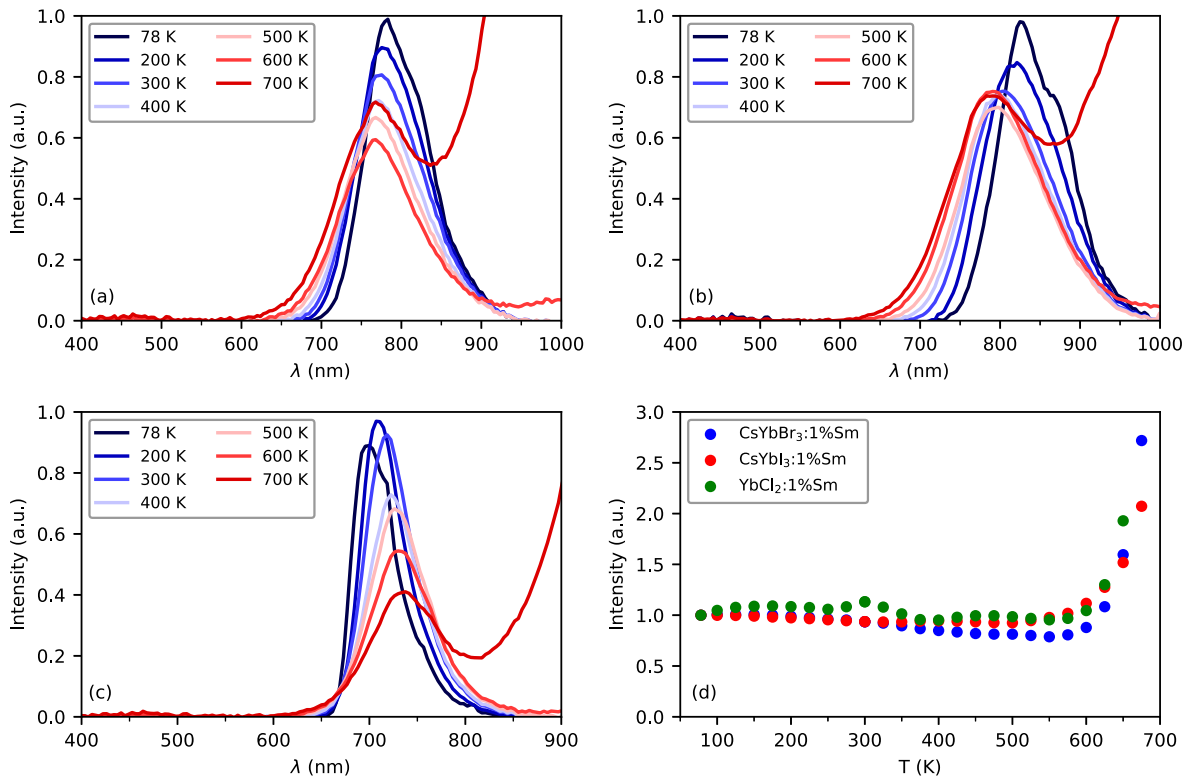

Fig. 2. X-ray excited emission spectra of (a) $CsYbBr_3$:1%Sm, (b) $CsYbI_3$:1%Sm and (c) $YbCl_2$:1%Sm. (d) Shows the emission intensity of all samples integrated from 600 nm to 1000 nm against temperature.

temperature is increased from 78 K to 700 K, the emission peak shifts from 790 nm to 765 nm. The strong increase in intensity at 700 K on the long wavelength side of the emission is due to blackbody radiation.

The X-ray excited luminescence spectra of CsYbI$_3$:1%Sm are shown in Fig. 2b. The sample displays a similar wide emission band as CsYbBr$_3$:1%Sm, which is therefore also attributed to the Sm^{2+} 4f^{5}5d → 4f^6 emission. In CsYbI$_3$:1%Sm, the Sm^{2+} emission is positioned at about 0.08 eV lower energy compared to CsYbBr$_3$:1%Sm. This is in accordance with the difference between the Eu^{2+} 4f^{6}5d → 4f^7 emission energy in CsCaI$_3$:Eu (2.86 eV) [34] and CsCaBr$_3$:Eu (2.78 eV) [33]. Just as in CsYbBr$_3$:1%Sm, the same shift of the Sm^{2+} emission to shorter wavelengths is observed when temperature is increased from 78 K to 700 K.

Fig. 2c shows the X-ray excited luminescence spectra of YbCl$_2$:1%Sm. The broad emission band between 650 nm and 850 nm is at about 60 nm shorter wavelength compared to CsYbBr$_3$:1%Sm and CsYbI$_3$:1%Sm. As opposed to the Sm^{2+} emission in CsYbBr$_3$:1%Sm and CsYbI$_3$:1%Sm, the Sm^{2+} emission in YbCl$_2$:1%Sm shifts to longer wavelengths when temperature is increased.

Fig. 2d shows the emission intensity of all samples integrated from 600 nm to 1000 nm, normalised to the intensity at 78 K. The emission intensity is almost perfectly stable between 78 K and 600 K. The sudden increase at temperatures above 600 K is caused by blackbody radiation overlapping with the Sm^{2+} emission. From Fig. 2a–c it can be seen that even at temperatures up to 700 K, the Sm^{2+} emission does not quench.

The X-ray excited decay curves of all samples are shown in Fig. 3. The decay curves of CsYbBr$_3$:1%Sm (Fig. 3a) and CsYbI$_3$:1%Sm (Fig. 3b) are fitted with single exponentials with decay times of 2.1 μs and 2.3 μs, respectively. Similar decay times were observed for Sm^{2+} emission in CsBa$_2$I$_5$:Sm [18] and SrI$_2$:Sm [17]. It is fast enough for γ-ray spectroscopy as over 99% of the scintillation light is emitted within 10 μs after excitation.

The decay curve of YbCl$_2$:1%Sm (Fig. 3c) is fitted with a double exponential decay function. The fast component contains 7% of the scintillation light and has a 0.7 μs day time. The remaining 93% of the scintillation light is emitted in a slow component with decay time of 4.3 μs? With this decay time, 10% of the scintillation light is emitted more than 10 μs after excitation, making the scintillator rather slow for use in γ-ray spectroscopy.

The scintillation performance of the samples was assessed by recording ^{137}Cs excited pulse height spectra with the scintillator crystals coupled to an APD. Only for CsYbI$_3$:1%Sm a photopeak was observed. The result is shown in Fig. 4a. The x-axis shows the number of primary electron hole pairs created in the APD, which corresponds to the number of photons detected in a scintillation event. In addition to scintillation events, the pulse height spectrum also contains a background of events that originate from the absorption of γ-rays directly in the APD. This background has been roughly approximated with an exponential function, which is depicted by the dotted line. Fig. 4b shows the pulse height spectrum where this background is subtracted, allowing for easier determination of the energy resolution. Around 20,000 photons are detected in scintillation events that fall in the 662 keV photopeak. The set-up has a quantum efficiency close to 100% at the emission wavelength of CsYbI$_3$:1%Sm [14], therefore the light yield of CsYbI$_3$:1%Sm is estimated to be 30,000 ph/MeV. The FWHM of the photopeak is around 7%.

The photoluminescence emission and excitation spectra of CsYbBr$_3$:1%Sm and CsYbI$_3$:1%Sm at 10 K are shown in Fig. 5a and b. They show the same Sm^{2+} emission as the spectra made under X-ray excitation (Fig. 2). The slight change in shape of the Sm^{2+} 4f^{5}5d → 4f^6 emission is predominantly caused by the difference in temperature and detector quantum efficiency. The excitation spectrum of the Sm^{2+} emission in both samples displays a shoulder on the long wavelength side of the excitation band around 650 nm. This is often observed as the transition from the Sm^{2+} 4f^6 ground state to the lowest 4f^{5}5d state has a lower oscillator strength than the transition to the 4f^{5}5d states that lie at slightly higher energy. Following the notation used by Wood and Kaiser,
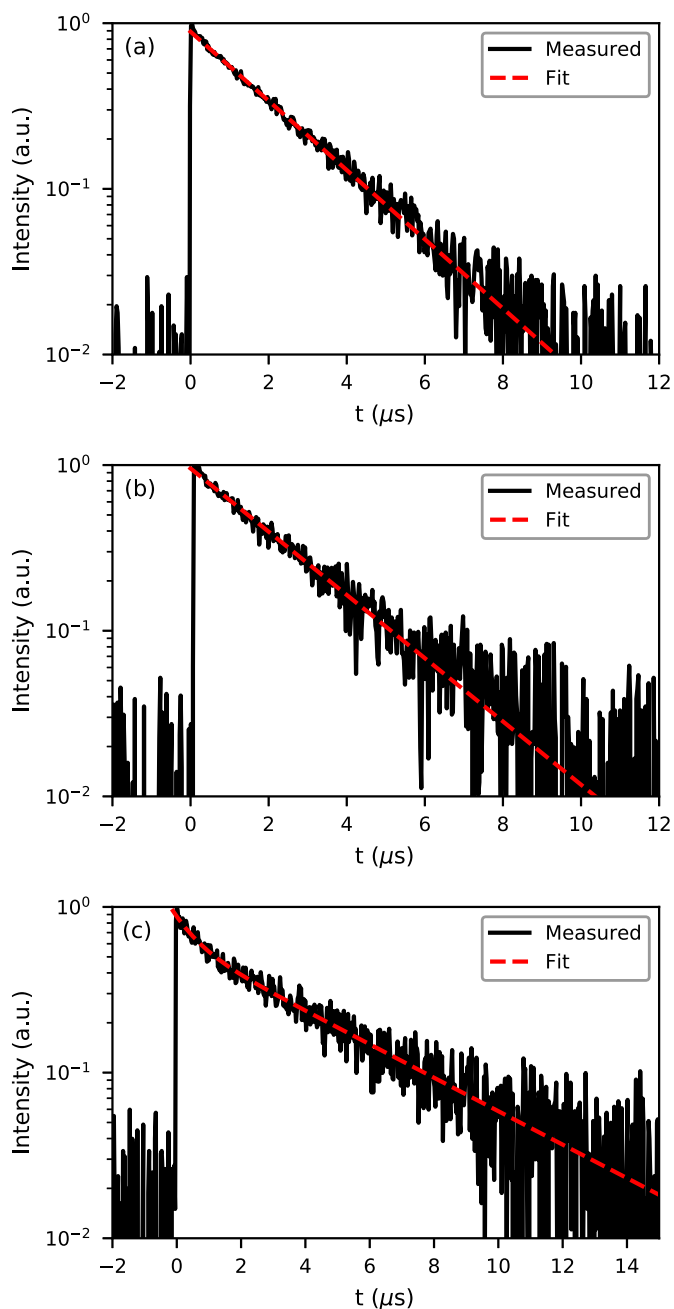

Fig. 3. X-ray excited decay curves of (a) CsYbBr$_3$:1%Sm, (b) CsYbI$_3$:1%Sm and (c) YbCl$_2$:1%Sm.

the shoulder and main excitation band are labelled the Sm A and B bands, respectively [35].

Due to the high Yb^{2+} concentration, it is expected that where Yb^{2+} absorbs, the Sm^{2+} excitation bands are not visible in the excitation spectrum. In CsCaBr$_3$:Yb and CsCaI$_3$:Yb, the lowest spin-allowed 4f^{14} → 4f^{13}5d excitation band of Yb^{2+} is located at 385 nm and 400 nm, respectively [36]. Based on this, the excitation bands between 250 nm and 400 nm are assigned to the 4f^{14} → 4f^{13}5d transitions of Yb^{2+} for both CsYbBr$_3$:1%Sm and CsYbI$_3$:1%Sm. The position of these excitation bands for CsYbI$_3$:1%Sm is in good agreement with the excitation bands of the intrinsic emission of CsYbI$_3$ measured by Zhao et al. [37] All bands at wavelengths longer than 400 nm are assigned to 4f^6 → 4f^{5}5d transitions of Sm^{2+}.

The emission spectrum of YbCl$_2$:1%Sm (Fig. 5c) contains exclusively Sm^{2+} 4f^6 → 4f^6 emission at 10 K (solid line), while at 300 K the emission
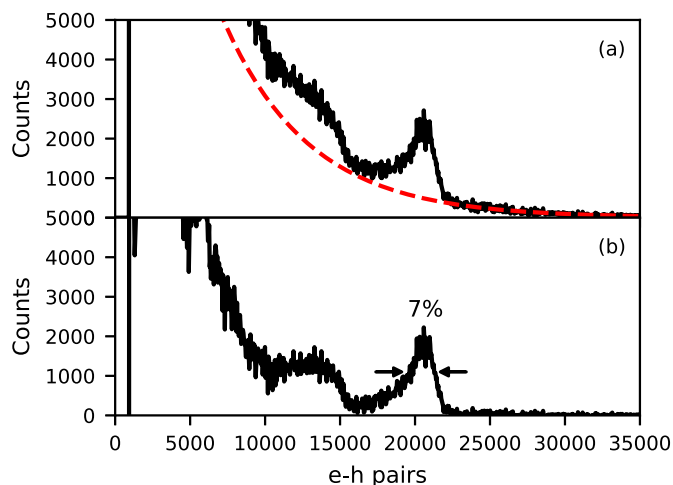
Fig. 4. Pulse height spectrum of CsYbI$_3$:1%Sm coupled to an APD using a ^{137}Cs γ-ray source. (a) Shows the pulse height spectrum as recorded, the red dashed curve indicates an approximate background due to direct γ-ray absorption in the APD, (b) shows the pulse height spectrum after subtraction of the background.

spectrum (dotted line) is entirely 4f^{5}5d → 4f^6 emission. This is caused by the 4f^{5}5d → 4f^6 emission wavelength of 720 nm being close to the turning point where Sm^{2+} shows exclusively line emission at all temperatures [25]. The excitation spectrum of Sm^{2+} emission in YbCl$_2$:1% Sm emission does not show a detailed structure as CsYbBr$_3$:1%Sm and CsYbI$_3$:1%Sm. In this sample, Yb^{2+} and Sm^{2+} are on a site of low symmetry. The crystal field splitting into five separate 5d levels causes the excitation bands of Sm^{2+} to smear over the entire optical spectrum, similar to what is observed in SrI$_2$:Sm [16,38]. The excitation spectrum does not show a resolved Sm A band. Based on the wavelength of the Sm B excitation band, it is estimated that Yb^{2+} starts to absorb around 370 nm.

Upon X-ray excitation, it is unclear what excitation mechanism is most prevalent. Electrons can be excited across the band gap, leaving a hole in the valence band. The small optical band gap of these materials also allows for excitation from the 4f^{14} ground state of Yb^{2+} to the conduction band. Eventually, the resulting ionisation should lead to excitation of Sm^{2+}. However, as the Yb^{2+} concentration is much higher than the Sm^{2+} concentration, it is likely that primarily Yb^{2+} is excited and the energy is then transferred to Sm^{2+}. In order to gain insight in the energy transfer from Yb^{2+} to Sm^{2+}, photoluminescence decay curves were measured upon excitation of the divalent lanthanides.

Fig. 6 shows the photoluminescence decay monitoring the Sm^{2+} emission of (a) CsYbBr$_3$:1%Sm, (b) CsYbI$_3$:1%Sm and (c) YbCl$_2$:1%Sm. The excitation wavelengths are chosen such that a decay trace is recorded when only Sm^{2+} is excited (red curves) and one where almost only Yb^{2+} is excited (blue curves). Even when exciting Yb^{2+}, the Sm^{2+} decay in all 3 compounds is at maximum intensity promptly after excitation. No components with rise time or long decay times are detected. The photoluminescence decay time of CsYbBr$_3$:1%Sm (2.1 μs) and CsYbI$_3$:1%Sm (2.2 μs) correspond well to the decay times under X-ray excitation, as was shown in Fig. 3. The photoluminescence decay time of YbCl$_2$:1%Sm is 5.2 μs, which is slower than the 4.3 μs day component that was observed under X-ray excitation. Whether this difference is caused by self-absorption, quenching or energy transfer is at this stage not known.

4. Discussion

To gain insight in the scintillation mechanism of CsYbBr$_3$:1%Sm, CsYbI$_3$:1%Sm and YbCl$_2$:1%Sm, vacuum referred binding energy (VRBE) diagrams are shown in Fig. 7. The energy of the divalent
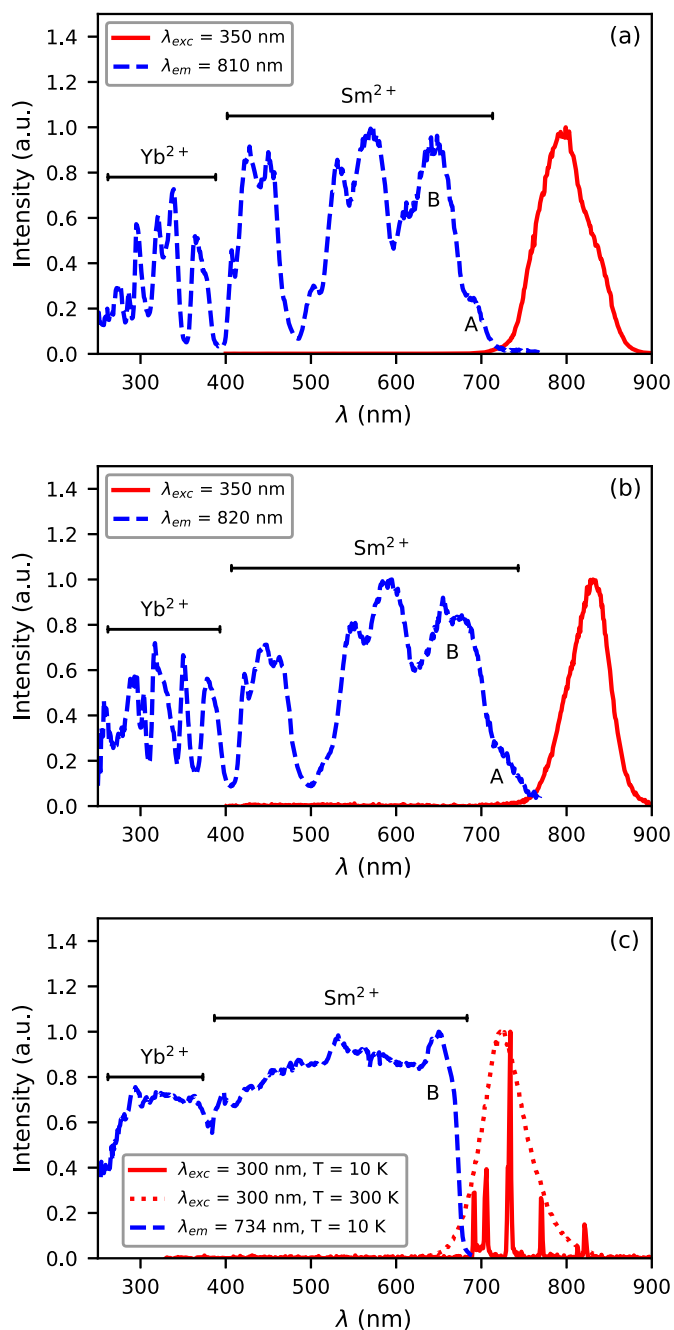

Fig. 5. Photoluminescence excitation and emission spectra of (a) CsYbBr$_3$:1% Sm, (b) CsYbI$_3$:1%Sm and (c) YbCl$_2$:1%Sm.

lanthanide 4f^n ground states is determined by the Eu Coulomb parameter $U(A)$, the tilt parameter $\alpha(A)$ and the nephelauxetic parameter $\beta(2+,A)$, as previously described by Dorenbos [39]. The values of these parameters have been estimated using typical values for compounds with similar anion types [39]. The spectroscopic data of Sm^{2+} presented in this article was used to place the 4f^{n-1}5d excited states ($E_{5d}(5,2+,A)$) with respect to the 4f^n ground states. The top of the valence band E_V was also estimated with typical values for compounds with the same anion type [40]. Lastly, the bottom of the conduction band E_C was placed 1 eV above the Sm^{2+} 4f^{5}5d level, which is estimated from the quenching temperature that lies above 700 K. All parameters used to create the VRBE diagram are provided in Table 1.

The energy of the valence band maximum is highly dependent on anion type, typically reducing the band gap from around 8 eV for
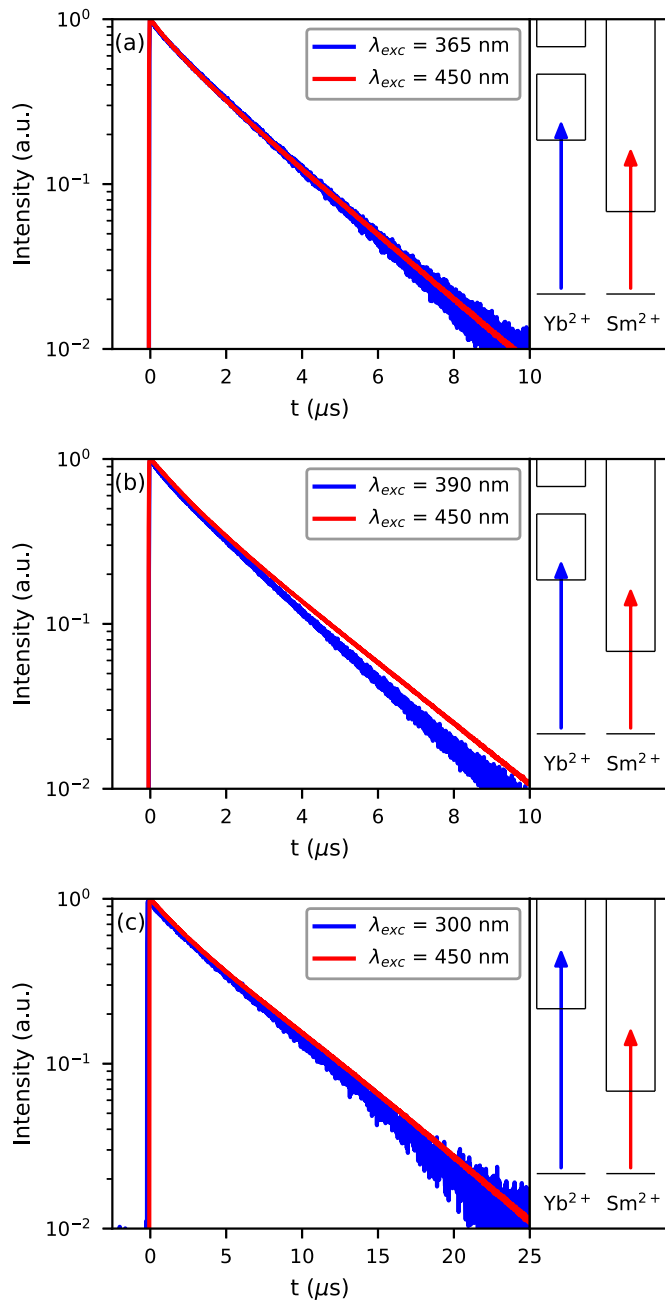
Fig. 6. Photoluminescence decay curves of (a) CsYbBr$_3$:1%Sm observed at 800 nm, (b) CsYbI$_3$:1%Sm observed at 800 nm, (c) YbCl$_2$:1%Sm observed at 720 nm. The right side of the figures shows schematically what transitions are excited, only the 4f ground state and 5d excited states are drawn. In CsYbBr$_3$:1%Sm and CsYbI$_3$:1%Sm (a and b), the two Yb^{2+} excited states indicate the 4f^{13}[^{2}F$_{7/2}$]5d and 4f^{13}[^{2}F$_{5/2}$]5d states.

Fig. 7. VRBE diagrams of (a) CsYbBr$_3$, (b) CsYbI$_3$ and (c) YbCl$_2$. The dark grey horizontal lines indicate the 4f^{14} ground state and 4f^{13}[^{2}F$_{7/2}$]5d$_1$ excited states and are drawn to indicate that Yb^{2+} is part of the host compound.

chlorides to nearly 5 eV for iodides. However, due to the high concentration of Yb^{2+}, the optical band gap in all these samples is determined by the Yb^{2+} 4f^{14} → 4f^{13}[^{2}F$_{7/2}$]5d$_1$[LS] transition, which is approximately 3.2 eV in all samples. The minimum energy required to excite an electron is thereby greatly reduced, allowing for an increase in the number of electron-hole pairs created in a scintillation event. The valence band consists of the np orbitals (n = 3–5) of the halide anions, meaning there are 3 * 6 = 18 valence band electrons for every 14 Yb^{2+} 4f electrons in CsYbBr$_3$ and CsYbI$_3$. In YbCl$_2$, there are 2 * 6 = 12 valence band electrons for every 14 Yb^{2+} 4f electrons. In a scintillation event an energetic primary electron excites bound electrons into the conduction band. When assuming equal probability for excitation of a valence band
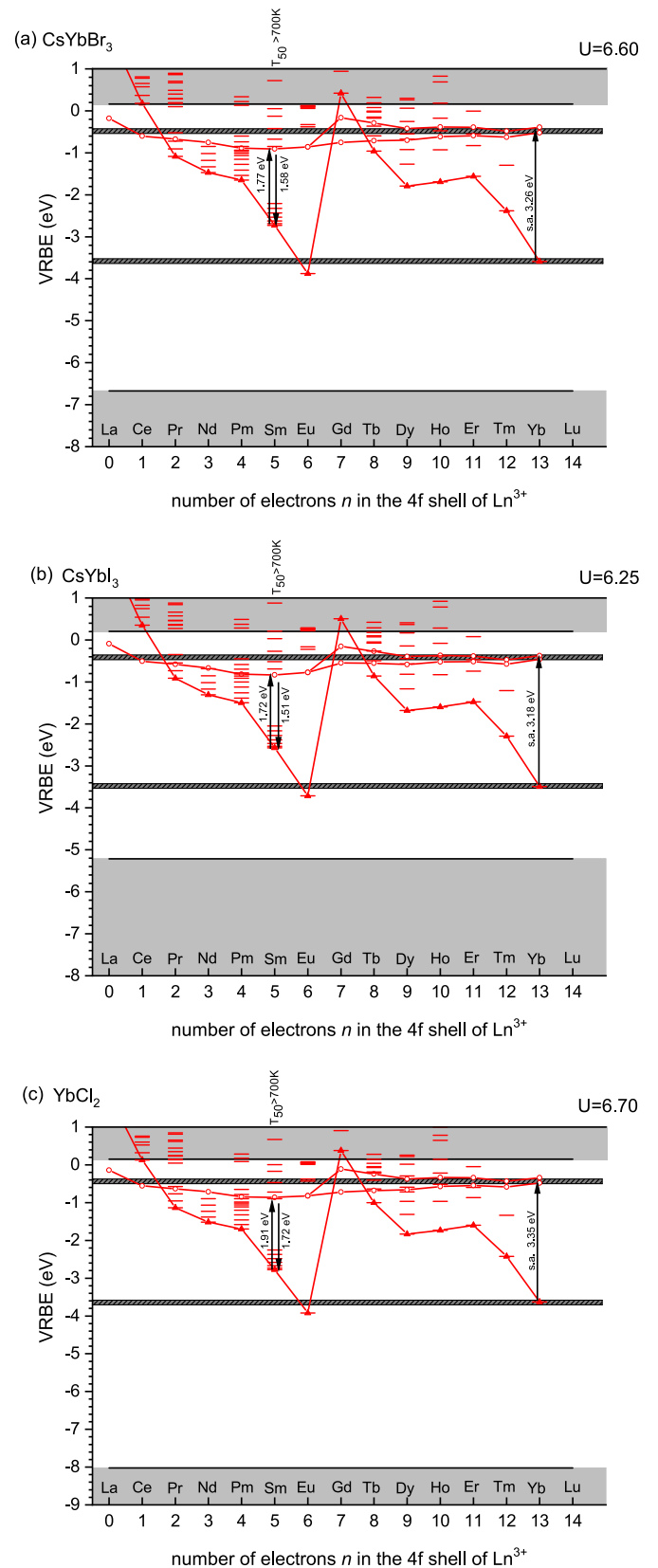
Table 1

Parameters used to construct the VRBE diagrams in Fig. 7.

Compound A	CsYbBr$_3$	CsYbI$_3$	YbCl$_2$
$U(A)$	6.67	6.25	6.70
$\alpha(A)$	0.095	0.095	0.095
$\beta(2+,A)$	0.92	0.91	0.92
$E^{5d}(5,2+,A)$	−0.9	−0.8	−0.9
$E_V(A)$	−6.7	−5.2	−8.0
$E_C(A)$	0.2	0.2	0.1

electron across the band gap or Yb^{2+} 4f^{14} electron into the conduction band, the average energy required to excite an electron in these materials can be calculated. This average energy will be labelled the effective band gap $E_{G\text{-eff}}$ in this work. The energies that correspond to the band gap (E_G), 4f^{13}[^{2}F$_{7/2}$]5d$_1$[LS] (E_{df}^{Yb2+}) and $E_{G\text{-eff}}$ are shown in Table 2.

The theoretical light yield limit Y_{th} in photons/MeV is defined by equation (3).

$$Y_{\text{th}} = \frac{10^6}{\beta E_G} \tag{3}$$

with β a value between 2 and 3. For the samples discussed in this work, Y_{th} is calculated using the $E_{G\text{-eff}}$ instead of E_G, the values are also shown in Table 2. Even though the estimated value of E_G is 1.2 eV larger for YbCl$_2$ than for CsYbBr$_3$, the higher atomic percentage of Yb^{2+} in YbCl$_2$ compared to CsYbBr$_3$ makes the value of Y_{th} almost identical for the two samples. Y_{th} has a value of 69,000–104,000 ph/MeV for CsYbI$_3$:1%Sm. However, the pulse height spectrum in Fig. 4 shows that 20,000 photons are detected after photoelectric absorption of a 662 keV γ-ray, which corresponds to a light yield of only 30,000 ph/MeV. Apparently the electron-hole pairs are transferred to Sm^{2+} with low efficiency.

In CsBa$_2$I$_5$:Yb,Sm, a loss of light yield was found to be caused by slow energy transfer from the Yb^{2+} 4f^{13}[^{2}F$_{7/2}$]5d$_1$[HS] state to Sm^{2+} [27]. The Yb^{2+} spin-forbidden 4f^{13}[^{2}F$_{7/2}$]5d$_1$[HS] → 4f^{14} emission showed photoluminescence decay time of around 100 μs? The Sm^{2+} photoluminescence decay showed a slow component with the same 100 μs day time. Additionally, the much faster energy transfer from the Yb^{2+} 4f^{13}[^{2}F$_{7/2}$]5d$_1$[LS] state resulted in a component with rise time in the Sm^{2+} emission. These energy transfer rates were a consequence of the relatively low concentrations of Yb^{2+} (2%–5%) and Sm^{2+} (0.5%–1%) that were used in the CsBa$_2$I$_5$ samples, which meant energy transfer from Yb^{2+} to Sm^{2+} took place through long range dipole-dipole interactions.

Compared to the previously studied CsBa$_2$I$_5$:Yb, Sm samples, the Yb^{2+} concentration in the samples discussed in this work is much higher. All samples show exclusively Sm^{2+} emission under X-ray excitation (Fig. 2). No Yb^{2+} or other host related emission is observed. Additionally, the X-ray excited decay profiles (Fig. 3) show that the Sm^{2+} emission is at maximum intensity promptly after excitation and no slow component is observed. This indicates that Yb^{2+} excitations are able to rapidly migrate through the lattice, facilitating fast energy transfer to Sm^{2+}. This is further confirmed by the photoluminescence decay curves in Fig. 6, where even upon excitation of Yb^{2+}, the maximum intensity of the Sm^{2+} emission is reached without any delay. By increasing the Yb^{2+} concentration to 99%, the light yield losses due to slow energy transfer from Yb^{2+} to Sm^{2+} have been solved. However, as indicated by the lower light yield than would theoretically be achievable in CsYbI$_3$:1% Sm, light yield losses still occur between creation of electron-hole pairs and subsequent excitation of Sm^{2+}.

5. Conclusions

The scintillation properties of CsYbBr$_3$:1%Sm, CsYbI$_3$:1%Sm and YbCl$_2$:1%Sm have been evaluated. All samples show exclusively Sm^{2+} 4f^{5}5d → 4f^6 emission under X-ray excitation which does not quench until temperatures higher than 700 K. The scintillation decay times are 2.1 μs, 2.3 μs and 4.6 μs for CsYbBr$_3$:1%Sm, CsYbI$_3$:1%Sm and YbCl$_2$:1%

Table 2

Energies of the (estimated) band gap E_G, the Yb^{2+} 4f^{14} → 4f^{13}[^{2}F$_{7/2}$]5d$_1$[LS] transition E_{df}^{Yb2+}, the effective band gap $E_{G\text{-eff}}$ and the theoretical light yield limit Y_{th}.

Compound A	CsYbBr$_3$	CsYbI$_3$	YbCl$_2$
E_G (eV)	6.9	5.4	8.1
E_{df}^{Yb2+} (eV)	3.26	3.18	3.35
$E_{G\text{-eff}}$ (eV)	5.7	4.8	6.0
Y_{th} (ph/MeV)	58,000–88,000	69,000–104,000	56,000–83,000

Sm, respectively. The decay curves show that Sm^{2+} reaches maximum intensity promptly after excitation and no slow component has been observed. Increasing the Yb^{2+} concentration to 99% has thus been shown to be an effective way to enable fast energy transfer from Yb^{2+} to Sm^{2+}. The ^{137}Cs excited pulse height spectrum of CsYbI$_3$:1%Sm coupled to an avalanche photodiode resulted in a photopeak with energy resolution of 7%. The light yield of CsYbI$_3$:1%Sm was estimated at 30,000 ph/MeV.

Author statement

Casper van Aarle was responsible for performing the experiments, writing the manuscript, preparing the figures and literature research. Karl W. Krämer was responsible for the materials and reviewing and editing the manuscript. Pieter Dorenbos was responsible for reviewing and editing the manuscript.

Declaration of competing interest

The authors declare that they have no known competing financial interests or personal relationships that could have appeared to influence the work reported in this paper.

Data availability

Data will be made available on request.

References

[1] Marvin J. Weber, J. Lumin. 100 (2002) 35.
[2] Pieter Dorenbos, Opt. Mater. X 1 (2019), 100021.
[3] M.S. Alekhin, J.T.M. de Haas, I.V. Khodyuk, K.W. Krämer, P.R. Menge, V. Ouspenski, P. Dorenbos, Appl. Phys. Lett. 102 (2013), 151915.
[4] L.A. Boatner, J.O. Ramey, J.A. Kolopus, R. Hawrami, W.M. Higgins, E. van Loef, J. Glodo, K.S. Shah, Emmanuel Rowe, Pijush Bhattacharya, Eugene Tupitsyn, Michael Groza, Arnold Burger, N.J. Cherepy, S.A. Payne, J. Cryst. Growth 312 (2010) 1213.
[5] Yuntao Wu, Li Qi, J.Rutstrom Daniel, Greeley Ian, Stand Luis, Loyd Matthew, Koschan Merry, L. Melcher Charles, Nucl. Instrum. Meth. A 954 (2020), 161242.
[6] Nerine J. Cherepy, Giulia Hull, Alexander D. Drobshoff, Stephen A. Payne, Edgar van Loef, Cody M. Wilson, Kanai S. Shah, Utpal N. Roy, Arnold Burger, Lynn A. Boatner, Woon-Seng Choong, William W. Moses, Appl. Phys. Lett. 92 (2008), 083508.
[7] Mikhail S. Alekhin, Daniel A. Biner, Karl W. Krämer, Pieter Dorenbos, J. Lumin. 145 (2014) 723.
[8] E.D. Bourret-Courchesne, G. Bizarri, R. Borade, Z. Yan, S.M. Hanrahan, G. Gundiah, A. Chaudhry, A. Canning, S.E. Derenzo, Nucl. Instrum. Methods A 612 (2009) 138.
[9] U. Shirwadkar, R. Hawrami, J. Glodo, E.V.D. van Loef, K.S. Shah, IEEE Trans. Nucl. Sci. 60 (2013) 1011.
[10] Jarek Glodo, V. Edgar, van Loef, Nerine J. Cherepy, Stephen A. Payne, Kanai S. Shah, IEEE Trans. Nucl. Sci. 57 (2010) 1228.
[11] Mikhail S. Alekhin, Karl W. Krämer, Pieter Dorenbos, Nucl. Instrum. Methods A 714 (2013) 13.
[12] Yuntao Wu, Mariya Zhuravleva, Adam C. Lindsey, Merry Koschan, Charles L. Melcher, Nucl. Instrum. Methods A 820 (2016) 132.

[13] Daniel Rutstrom, Luis Stand, Merry Koschan, Charles L. Melcher, Mariya Zhuravleva, J. Lumin. 216 (2019), 116740.
[14] T. M. de Haas Johan, Pieter Dorenbos, IEEE Trans. Nucl. Sci. 55 (2008) 1086.
[15] M. Guzzi, G. Baldini, J. Lumin. 6 (1973) 270.
[16] Mikhail S. Alekhin, H. Roy, P. Awater, Daniel A. Biner, Karl W. Krämer, T. M. de Haas Johan, Pieter Dorenbos, J. Lumin. 167 (2015) 347.
[17] R.H.P. Awater, M.S. Alekhin, D.A. Biner, K.W. Krämer, P. Dorenbos, J. Lumin. 212 (2019) 1.
[18] Weronika Wolszczak, Karl W. Krämer, Pieter Dorenbos, Phys. Status Solidi R. 13 (2019), 1900158.
[19] W. Wolszczak, K.W. Krämer, P. Dorenbos, J. Lumin. 222 (2020), 117101.
[20] E. Rowe, E. Tupitsyn, B. Wiggins, P. Bhattacharya, L. Matei, M. Groza, V. Buliga, A. Burger, P. Beck, N.J. Cherepy, S.A. Payne, Cryst. Res. Technol. 48 (2013) 227.
[21] Kohei Mizoi, Miki Arai, Yutaka Fujimoto, Daisuke Nakauchi, Masanori Koshimizu, Takayuki Yanagida, Keisuke Asai, J. Lumin. 227 (2020), 117521.
[22] Kohei Mizoi, Miki Arai, Yutaka Fujimoto, Daisuke Nakauchi, Masanori Koshimizu, Takayuki Yanagida, Keisuke Asai, J. Ceram. Soc. Jpn. 129 (2021) 406.
[23] Daniel Rutstrom, Luis Stand, Bogdan Dryzhakov, Merry Koschan, L. Charles, Melcher, Mariya Zhuravleva, Opt. Mater. 110 (2020), 110536.
[24] Sekine Dai, Yutaka Fujimoto, Masanori Koshimizu, Daisuke Nakauchi, Takayuki Yanagida, Keisuke Asai, Jpn. J. Appl. Phys. 59 (2020), 012005.
[25] P. Dorenbos, J. Phys. Condens. Matter 15 (2003) 575.
[26] Markus Suta, Tim Senden, Olchowka Jacob, Matthias Adlung, Andries Meijerink, Claudia Wickleder, Phys. Chem. Chem. Phys. 19 (2017) 7188.
[27] Casper van Aarle, Karl W. Krämer, Pieter Dorenbos, J. Lumin. 238 (2021), 118257.
[28] D.L. Dexter, J. Chem. Phys. 21 (1953) 836.
[29] Gaby Schilling, Z. Gerd Meyer, Anorg. Allg. Chem. 662 (1992) 759.
[30] Markus Suta, Claudia Wickleder, Adv. Funct. Mater. 27 (2017), 1602783.
[31] Christine A. Voos-Esquivel, Harry A. Eick, J. Solid State Chem. 67 (1987) 291.
[32] G. Meyer, Advances in the Synthesis and Reactivity of Solids, vol. 2, JAI Press Inc., 1994, pp. 1–16.
[33] M. Suta, P. Larsen, F. Lavoie-Cardinal, C. Wickleder, J. Lumin. 149 (2014) 35.
[34] Markus Suta, Claudia Wickleder, J. Mater. Chem. C 3 (2015) 5233.
[35] D.L. Wood, W. Kaiser, Phys. Rev. 126 (1962) 2079.
[36] Markus Suta, Wener Urland, Claude Daul, Claudia Wickleder, Phys. Chem. Chem. Phys. 18 (2016), 13196.
[37] Xinhua Zhao, Yongzhi Deng, Zhonghe Li, Shishua Wang, J. Alloys Compd. 250 (1997) 405.
[38] Mirosław Karbowiak, Piotr Solarz, Radosław Lisiecki, Witold Ryba-Romanowski, J. Lumin. 195 (2018) 159.
[39] Pieter Dorenbos, J. Lumin. 222 (2020), 117164.
[40] Pieter Dorenbos, J. Lumin. 136 (2013) 122.